Optical and Quantum Electronics (2022) 54:394
https://doi.org/10.1007/s11082-022-03783-9

Spatiotemporal dynamics of self-similar parabolic pulse evolution in multimode fibers

Leila Graini[1,2] · **Bülend Ortaç**[2]

Received: 11 February 2022 / Accepted: 28 April 2022 / Published online: 5 June 2022

Abstract
In this paper, we have investigated for the first time, the spatiotemporal dynamics of self-similar parabolic pulse evolution in multimode fibers. Two types of fiber are considered, graded-index and step-index MMFs. For the quality of the generated parabolic pulse, the mismatch parameter is used. A thorough study of the evolution of the pulse parameters as a function of the initial parameters has been carried out. As a result, the initial pulse evolved into a linearly chirped pulse with a parabolic intensity shape in both fibers, under the predominantly excitation of the fundamental mode. It has been shown, in particular, that the pulse can be compressed to a temporal duration of about 40 fs. Moreover, a spatiotemporal nonlinear dynamic, beam auto-selection, of one specific mode, is investigated through graded-index MMF, under the different initial modes excitation. The parabolic pulse formation process plays a critical role in this nonlinear dynamic. This approach provides another framework to understand the complex nonlinear dynamics in MMFs.

Keywords Multimode fibers · Spatiotemporal parabolic pulse · Self-similar propagation · Beam auto-selection

1 Introduction

Self-similar parabolic pulse generation in single-mode fibers (SMFs), first predicted in 1993 by Anderson et al. (1993) and then demonstrated in 2000 by Fermann et al. (2000), has been widely investigated and is still an active area of research due to its unique characteristics and numerous applications for potential scaling approach of fiber laser systems to unprecedented pulse energy and power levels (Kruglov et al. 2002; Hirooka and Nakazawa 2004; Finot et al. 2006, 2007; Boscolo et al. 2008; Ghosh et al. 2009; Iakushev et al. 2012; Biswas et al. 2016; Liu et al. 2017; Chowdhury et al. 2019; Schukarev et al. 2019). Such

✉ Leila Graini
graini.leila@univ-guelma.dz

Bülend Ortaç
ortac@bilkent.unam.edu.tr

[1] Telecommunications Laboratory, 8 Mai 1945-Guelma University, 24000 Guelma, Algeria

[2] National Nanotechnology Research Center and Institute of Materials Science and Nanotechnology, Bilkent University, 06800 Ankara, Turkey

pulse is an attractor solution to the nonlinear Schrödinger equation (NLSE) in a normal dispersion regime with the presence of nonlinearity. It is also presented robustness to the wave-breaking under high-intensity conditions, as well as its characteristic linear chirp can be lead to efficient pulse compression. However, utilizing SMFs for this purpose limits the improvement of output pulse energy, imposed by the small mode field area of SMFs. The use of MMFs, which incorporate an additional spatial degree of freedom, could overcome this limitation due to the larger mode field area. We can furthermore expect a particular interest in multimode parabolic pulses in the development of higher pulse energy and short-pulse sources, for different applications with controllable spatiotemporal properties.

MMFs have recently attracted huge attention as a testbed to investigate uncovered complex spatiotemporal dynamics such as spatiotemporal solitons, modulation instability, supercontinuum generation, self-similar fiber laser, and mode-locking multimode fiber laser (Ahsan and Agrawal 2018; Teğin and Ortaç 2017, 2018; Teğin et al. 2019; Wright et al. 2020). On the contrary, the spatiotemporal dynamics of parabolic pulses in MMFs have seldom been studied, which arouses our interest. To the best of our knowledge, only one study has investigated parabolic pulse generation in exponentially tapered MMFs structure (Lopez Aviles et al. 2019). Actually, the tapered profile provides an equivalent gain similar to that of the Yb or Er-doped fibers (Hirooka and Nakazawa 2004), so that the passive generation of a parabolic pulse is possible. However, the multimode propagation regime is not considered, and so the spatiotemporal nonlinear dynamics are neglected, as well. Furthermore, the theoretical analysis is based on the simplified NLSE. Then, parabolic pulse generation and its spatiotemporal dynamics in uniform MMFs structures would be a question to investigate.

In this paper, based on the multimode generalized nonlinear Schrödinger equation (GMM-NLSE), we have presented numerical predictions of the existence of a parabolic pulse in MMFs. Graded and Step-index MMFs (GRIN-F and STEP-F) platforms are used. We consider first a GRIN-F, and the analysis is extended to two different initial conditions, mainly fundamental mode excitation and equal distribution of initial pulse energy among all the modes. The same analysis is then repeated for the STEP-F. Under the first initial condition, both MMFs behave as a SMFs and observe an attraction towards a parabolic waveform. The results show that the pulse evolved into a linearly chirped pulse with a well-matched parabolic intensity shape that propagates self-similarly. In addition, the spatial beam profile remains a Gaussian-like profile of the fundamental mode. However, under the second initial condition, the results were different between the GRIN-F and the STEP-F. Moreover, we have observed an interesting nonlinear phenomenon in the GRIN-F, beam auto-selection, represented by the evolution of the multimode spatial beam profile into a single-mode profile.

2 Numerical modeling of parabolic pulse generation in MMFs

The equation applied for the numerical simulation of nonlinear pulse propagation in passive MMFs is the GMM-NLSE (Poletti and Horak 2008), which is widely used in the numerical investigation to solve problems related to MMFs. The GMM-NLSE (1) is a system of coupled NLSE-type equations for the electric field temporal envelope for spatial mode p, which requires preliminary knowledge of the initial pulse energy distribution among the different spatial modes of the MMF. It is including the effects of stimulated Raman scattering, dispersion up to fourth order, self-steepening, and intermodal effects. We solve Eq. (1)

numerically using, the most popular, the fourth-order Runge–Kutta method (Hult 2007). Note that, Eq. (1) can be solved also by the adaptive step-size methods (Wen et al. 2019), witch more appropriate for short pulses up to 50 fs.

$$\begin{aligned}\partial_z A_p &= i\left(\beta_0^{(p)} - \Re\left[\beta_0^{(0)}\right]\right)A_p \\ &- \left(\beta_1^{(p)} - \Re\left[\beta_1^{(0)}\right]\right)\frac{\partial A_P}{\partial t} + i\sum_{n\geq 2}\frac{\beta_n^{(p)}}{n!}\left(i\frac{\partial}{\partial t}\right)^n A_p \\ &+ i\frac{n_{2\omega_0}}{c}\left(1+\frac{i}{\omega_0}\partial t\right)\sum_{l,m,n}\left\{(1-f_R)S^k_{plmn}A_l A_m A_n^* + f_R A_l S^R_{plmn}\int_{-\infty}^{t} d\tau A_m(z,t-\tau)A_n^*(z,t-\tau)h_R(\tau)\right\}\end{aligned} \tag{1}$$

where A_p is the electric field of mode p. The first three terms on the right-hand side are the result of approximating the dispersion operator in the mode p by a Taylor series expansion about ω_0, then transforming the terms into the time domain. $\beta_0^{(p)}$ are the propagation constants, $\beta_1^{(p)}$ are the modal dispersions, represent the walk-off among the spatial modes, and $\beta_n^{(p)}$ are the higher-order dispersion coefficients of mode p. $\Re[\ldots]$ denotes the real part only. The next terms represent the effects of optical nonlinearity with the nonlinear refractive index $n_2 = 3.2\times10^{-20}$ m^{2}W^{-1}. S^k_{plmn} and S^R_{plmn} are the mode coupling tensors for Kerr and Raman effects, respectively. They are proportional to the overlap integrals of the transverse modal field distributions, where p, l, m, and n represent the numbers of spatial modes. f_R is the fractional contribution of the Raman effect ($f_R = 0.18$). h_R is the delayed Raman response function. The model of the Eq. (1) couples the propagating mode fields via Kerr nonlinearities, self-phase modulation (SPM) corresponds to Terms S^k_{pppp} with effective areas of $A_{eff} = 1/S^K_{PPPP}$, for each spatial mode. Whereas, cross-phase modulation (XPM) corresponds to terms $1/S^k_{ppmn}$ and $1/S^k_{pnpn}$, with $n \neq p$. All other nonlinear coupling terms can be described as four-wave mixing (FWM), which are the terms that can cause the transfer of energy between modes. The spatial modes, dispersions, and nonlinear coupling coefficients are calculated from the MMFs specifications using the numerically-calculated modes for MMFs as implemented by Wright et al. (2018).

The MMFs under consideration are assumed to have a core radius of 25 μm, a parabolic and step refractive index profiles in the GRIN-F and the STEP-F, respectively, with index contrast $\Delta = 0.0068$ and numerical aperture NA = 0.17. These MMFs are excited at the wavelength of 1030 nm, where the dispersion is normal. Although both MMFs can support multiple modes at 1030 nm, to reduce the computational time, we only consider the first six linearly polarized modes (LP_{01}, LP_{11a}, LP_{11b}, LP_{21a}, $LP_{21b,}$ and LP_{02}) in our numerical studies. These modes would be excited most when we initially launch the pulse into only the fundamental LP_{01} mode (Wright et al. 2018).

The two fibers, even for similar specifications, present different characteristics in dispersion and nonlinearity coefficients. For the STEP-F, the values of the group-velocity dispersion $\beta_2^{(p)}$ of the six calculated spatial modes are in the range of 17.6–18.7 ps^2/km, and $\Delta\beta_1^{(p)}$ of modes 2–6 are 0.37, 0.37, 0.87, 0.87, and 1.05 ps/m, respectively. While, for the GRINF, $\beta_2^{(p)}$and $\Delta\beta_1^{(p)}$ are approximately 18.9 ps^2/km and 0.016 ps/m, respectively. It is worth noting, that the effective areas of modes (A_{eff}) in the STEP-F are larger than those in the GRIN-F (Poletti and Horak 2008) and, therefore, the variations in the nonlinear coefficients (γ) of modes in the GRIN-F are wider than those in the STEP-F. The values of A_{eff} and γ are 155.09 μm^2, 1.22 W^{-1} km^{-1} and 966.43 μm^2, 0.2 W^{-1} km^{-1} for the GRIN-F and the STEP-F, respectively. These values are scaling as of the fundamental modes (Mafi 2012).

To check the quality of the formed parabolic pulse, we used the misfit parameter (M) between the pulse's temporal intensity profiles A_p and a parabolic fit A_{fit} (Finot et al. 2006):

$$M_p^2 = \frac{\int \left(\left|A_p\right|^2 - \left|A_{fit}\right|^2 \right)^2 d\tau}{\int \left|A_P\right|^4 d\tau} \tag{2}$$

The expression for a parabolic pulse of energy $U_p 4P_p T_p/3\sqrt{2}$ is given by:

$$\begin{cases} A_p(T) = \sqrt{P_p}\sqrt{1 - 2T^2/T_p^2}\ exp\left(-iC_p T^2/2\right) & |T| \le T_p/\sqrt{2} \\ A_p(T) = 0, & |T| > T_p/\sqrt{2} \end{cases} \tag{3}$$

where P_p is the peak power of the parabolic pulse, T_p is the time duration and C_P is the linear chirp coefficient. The misfit parameter, M, allows estimating the pulse shape imperfection as compared to the parabolic shape. The low value of M shows a better fit to the parabolic waveform. We consider that the pulse shape is parabolic for $M \le 0.04$ (Finot et al. 2006).

3 Spatiotemporal parabolic pulse generation through the proposed GRIN-F

3.1 Under the condition of the predominant fundamental mode of excitation

In this simulation, we assume a Gaussian-shaped input pulse with a pulse duration of 200 fs propagates in 1 m of the proposed GRIN-F. The initial pulse energy is considered to be 7 nJ, corresponding to the peak power of about 35 kW. We set this energy mostly coupled in the fundamental LP_{01} mode as 99%. We consider weak excitation of the other modes, which could be the case in an experiment. The pulse evolution in the GRIN-F is depicted in Fig. 1 and explicitly shows the characteristics of the self-similar regime in both the temporal and spectral domains. The temporal and spectral widths increase exponentially, whereas, the amplitudes decrease with propagation inside the fiber. As the parabolic pulse reshaping inside the fiber is governed by the SPM and normal dispersion, two propagation regimes are observed, like that found in previous studies (Fermann et al. 2000; Kruglov et al. 2002; Ghosh et al. 2009). The first regime implies reshaping the pulse in a short propagation distance. In this part, the strong action of the SPM effect leads to a fast change of the pulse shape and its spectrum, with a nonlinear pulse chirp. In the second regime, the pulse profile converges to the parabolic shape and evolves in a self-similar manner. In this part, dispersion is more predominant than the SPM, which appeared by the large broadening of the pulse duration and the slow variation of the spectrum expansion that approaches its maximal, and the chirp becomes linear. It should be noted that, from the above results, no wave breaking or modulation instability sidebands are observed due to the proper selection of the launch conditions (pulse width, peak power, fiber core size, wavelength, etc.). However, this kind of nonlinear effect required higher peak power that breaks up the temporal waveform into a train of pulses (Teğin and Ortaç 2018).

Figure 2 displays the pulse characteristics after propagation inside 1 m GRIN-F length. As presented in Fig. 2a, the input pulse evolves towards a parabolic waveform with a

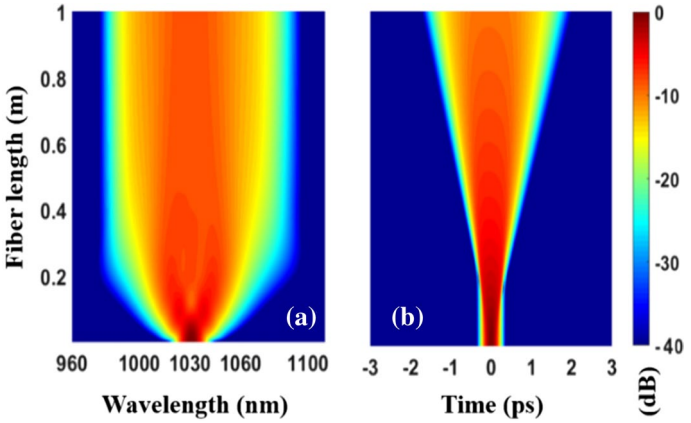

Fig. 1 Self-similar evolution of parabolic pulse for spectral (**a**) and temporal (**b**) domains in GRIN-F, where the initial energy is mostly coupled in the LP_{01} mode

quasi-linear chirp in the entire pulse duration of ~ 2 ps. The temporal profile of the parabolic pulse and the chirp are in good agreement with a parabolic fit and a theoretical chirp (black dashed line), respectively. The misfit parameter (M) is also calculated, using Eq. 2,

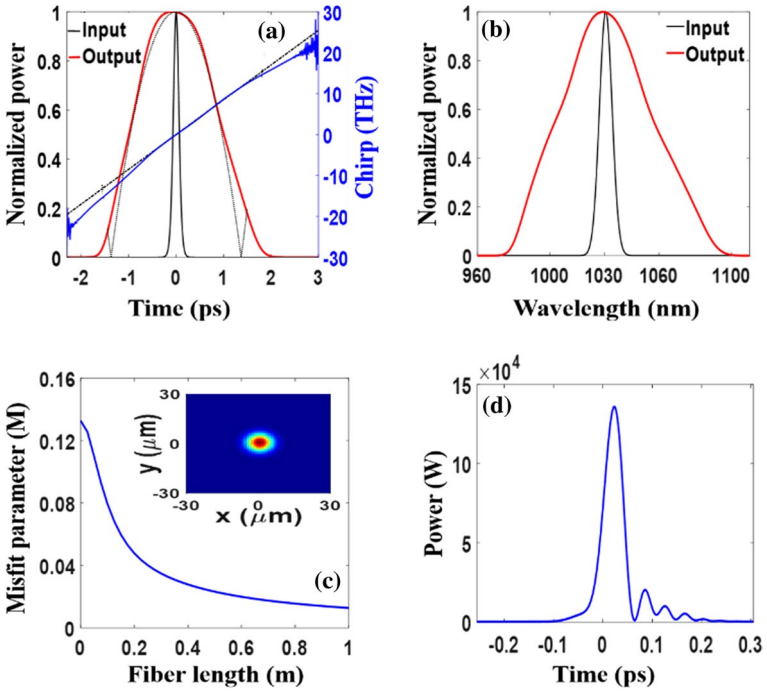

Fig. 2 The temporal (**a**) and the spectral (**b**) output form of the parabolic pulse in GRIN-F, where the initial energy is mostly coupled in the LP_{01} mode. The misfit parameter (M) evolution (**c**), and temporal form of the compressed pulse (**d**). (Inset: the spatial beam profile of the generated pulse)

to quantify the quality of the generated parabolic pulse. As it can be inferred from Fig. 2c, M reaches its minimum value of 0.013 at 1 m of propagation, and the pulse shape indeed is very close to the ideal parabolic waveform. The spatial beam profile of the total field following the pulse propagation over 1 m of GRIN-F is presented in the inset of Fig. 2c. As it can be seen, the Gaussian-like spatial profile of the LP_{01} mode is preserved along with the fiber. Consequently, we prove that the parabolic pulse is generated only in the LP_{01} mode so that energy transfer from the LP_{01} mode into the other modes is limited and the other modes are decoupled. In fact, the initial pulse energy of 7 nJ leads the pulse nonlinearity length (22.15 mm) to be longer than the minimum modal walk-off length (7.5 mm), in which modes coupling could be avoided since it is mainly limited to energy-dependent effects (Poletti and Horak 2008). The spectral evolution of the input pulse is also presented in Fig. 2b, showing that a substantial broadening of the spectrum with a bandwidth up to 60 nm is obtained. The above results imply that the parabolic pulse generated in the GRIN-F can be compressed in dispersive media down to 40 fs as presented in Fig. 2d so that a compression factor of 5 is obtained. Note that the pedestals on the compressed pulse are being observed. However, the energy presented in the pedestals is extremely low compared to that of the main lobe. We then estimated that 80% of the total energy is contained in the main lobe (~5.6 nJ), while 20% is in the pedestals of the compressed pulse (~1.4 nJ).

3.2 Under the condition of excitation by the equal energy distribution among all the modes

In this case, we first initialized simulation with the initial pulse energy equally distributed among all the modes. Indeed, such a configuration can be achieved in practice (Teğin et al. 2020). To avoid the strong nonlinear coupling between the modes, the initial pulse energy of 1.5 nJ is used. Other parameters are kept fixed. The corresponding results are depicted in Fig. 3. It is clearly seen that the initial pulse exhibits growth in time duration and spectral width while all the modes evolved towards the respective parabolic shapes, as shown in Fig. 3a and b, respectively. Additionally, the complex temporal profile and spectrum of the generated entire pulse are not deformed, and so a localized multimode pulse is achieved, owing to the fact that, the very small walk-off (0.016 ps/m) inside 1 m GRIN-F length, leads the modes to be well centered in the temporal and spectral domain. More interestingly, through all the modes, only LP_{01} and LP_{02} are significantly gain energy, due to the energy transfer that occurs between modes, as shown in Fig. 3d. Note that the energy transfer between two modes requires group velocity matching and a non-negligible nonlinear overlap integral (Poletti and Horak 2008). Furthermore, in GRIN.F, the modes fall into discrete groups and as such, they have identical group velocities in the same group (Wright et al. 2018). Thus, the initial energy transfers from the other modes into LP_{01} and LP_{02}, because the group velocity of LP_{01} matched with that of LP_{11a} and LP_{11b}, while the group velocity of LP_{02} matched with that of the LP_{11a}, LP_{11b}, $LP_{21a,}$ and LP_{21b} modes, which in turn leads to a difference of energy transfer efficiency between these modes. We have also displayed in Fig. 3c, the evolution of the Misfit parameters (M) for all the modes. We noticed that the minimum value of M is quite diverse, and depends on the energy of each mode. Notably, the M parameter increases considerably as the mode energy increases and leads to a deviation from the parabolic shape. This behavior can be explained that higher energy provides a stronger impact on SPM, and parabolic mode reshaping is relatively sufficient. Like in the case of LP_{02} mode, which gains energy, the M parameter is 0.039. On the other hand, in LP_{11a} mode, which lost energy, the dispersion dominates, and

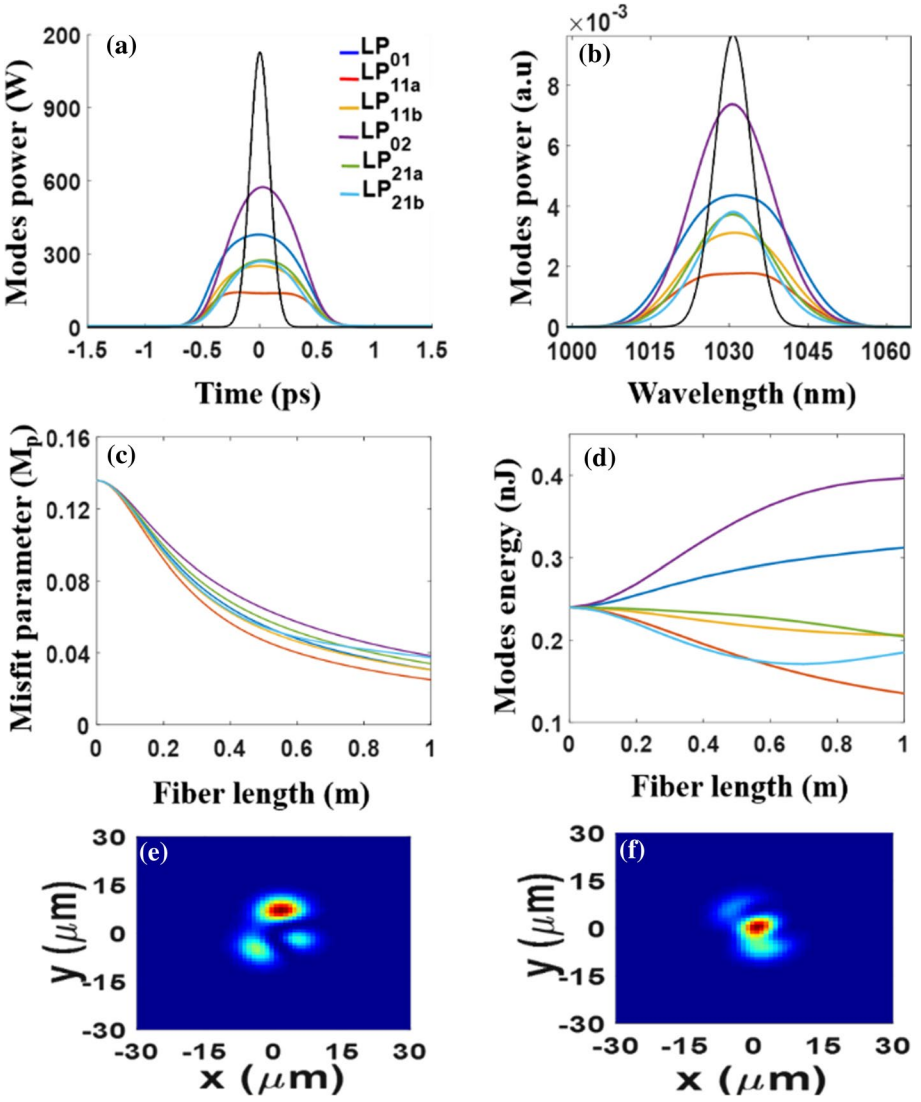

Fig. 3 The output power (**a**), the corresponding spectra (**b**), the misfit parameters (**c**), and the modal energy evolution (**d**) of all the modes. The input (**e**) and output (**f**) spatial beam profiles

parabolic mode reshaping occurs quickly with a better M parameter of 0.025. In addition, the required distance to achieve a parabolic shape with a good M parameter ($M < 0.04$) is varied among all the modes. These distances are 0.6 m for LP_{11a}, 0.8 m for LP_{01}, $LP_{11b,}$ and $LP_{21a,}$ and 1 m for LP_{02} and LP_{21b} modes, respectively. Besides, as it can be seen from Fig. 3d, the initial energy starts to transfer from the other modes into LP_{01} and LP_{02} at a distance of 0.1 m, and then, a steady-state is reached after ~ 0.9 m with 50% of the initial energy is presented in these modes (20% in LP_{01} and 30% in LP_{02}), leads the spatial beam profile of the input pulse, presented by the overlapped profile of all the modes, evolved

from a speckled pattern to a centered beam profile mainly composed by LP_{01} and LP_{02} modes dominating, as shown in Fig. 3e and f, respectively.

To investigate the origin of the spatial behaviors, we then varied the initial pulse energy. Other parameters are kept fixed. Figure 4 depicts the corresponding results with three initial pulse energy cases. We noted that even though the initial pulse energy is equally distributed among all the modes, the results revealed significant spatiotemporal differences entirely. As shown in Fig. 4a, at relatively low pulse energy less than 0.15 nJ (called linear propagation regime), the modes evolved without providing a parabolic reshaping and the corresponding output spatial beam profile is containing all the modes (inset of Fig. 4a).

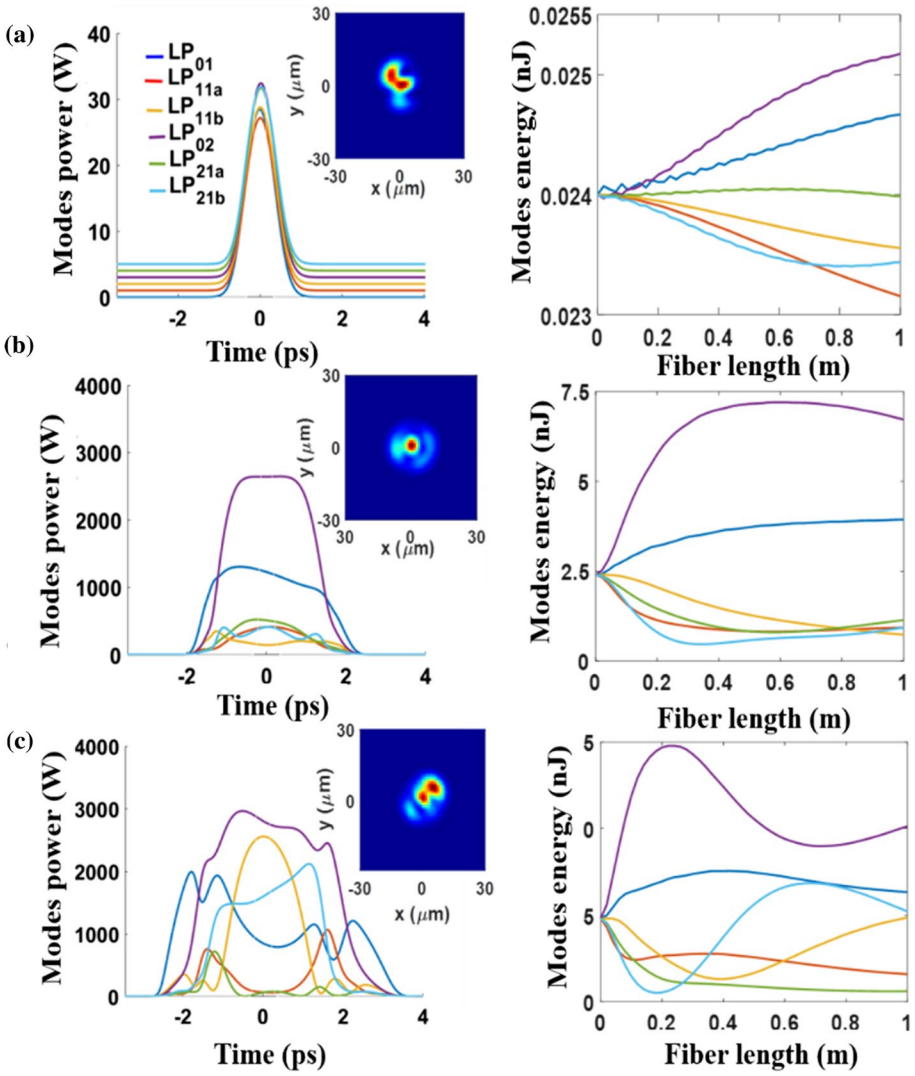

Fig. 4 The output power of all the modes (inset: output spatial beam profile) and the modal energy evolution for an initial pulse energy of 0.15 nJ (**a**),15 nJ (**b**), and 30 nJ (**c**)

Because the very weak energy transfer occurred between modes, the energy of each mode maintains almost the initial value with mode content remaining at ~ 17%. When the initial pulse energy is increased up to 15 nJ, significant energy transfer between modes is observed, owing to the group-velocity matching, which results in the transfer of 50% of the energy from the other modes to LP_{02} mode, and so it emerges and dominates, as shown in Fig. 4b. Besides, the LP_{01} mode gains less energy (~ 25%), whereas, the remaining energy is distributed roughly equally among the other modes. The energy evolution of LP_{02} mode toward a steady-state is reached at a distance of 0.4 m. This is consistent with the evolution of the parabolic pulse as it evolves toward the maximum before the break-up. More interestingly, the initial multimode beam profile (Fig. 3f) is evolved to a single-mode profile resembling that of the LP_{02} mode, as it is dominating (inset of Fig. 4b). This observation called beam auto-selection may be related to the self-organized nonlinear attraction to low-order modes, known as Kerr beam clean-up, which has been observed in many works both in the normal and anomalous dispersion regime of GRIN-Fs (Krupa et al. 2017; Zhanwei et al. 2016; Leventoux et al. 2020). Although beam clean-up has been mainly reported on the fundamental mode, it is obtained on higher-order modes as well, by properly managing the input coupling conditions (Deliancourt et al. 2019). Nonetheless, the beam clean-up has been investigated only where chromatic and modal dispersions do not play a role. On the opposite, the presence of both nonlinearity and normal dispersion is important for parabolic pulse generations. Note also that, the beam clean-up might be accompanied by a complex temporal pulses break-up and compressing the input pulses (Krupa et al. 2018). To see how parabolic pulse evolves during the follow-up process, we continue increasing the initial pulse energy. As shown in Fig. 4c, when the initial pulse energy is increased to up 30 nJ, the modes undergo significant evolution under energy exchange between them, owing to the strong modes coupling and group-velocity matching, resulting in the deterioration of modes towards parabolic waveforms. We note also that, in this case, there is no mode predominant over others, and the output spatial beam profile is containing all the modes with different amounts of energy (inset of Fig. 4c). These results prove that the parabolic pulse formation process, and the energy transfer between modes which induced by group velocity matching, could have a prominent effect on the spatiotemporal behavior inside the GRIN-F. Moreover, the occurrence of beam auto-selection on the LP_{02} mode remains spatial beam profile stable for more than a decade of initial pulse energy variation (from 1.5 to 15 nJ).

4 Spatiotemporal parabolic pulse generation through the proposed STEP-F

4.1 Under the condition of the predominant fundamental mode of excitation

Similar to the case of the GRIN-F, we assume a Gaussian-shaped input pulse with a pulse duration of 200 *fs* propagates in 1 m of STEP-F. The initial pulse energy is considered to be 50 nJ (peak power is 250 kW). We set this energy mostly coupled in the LP_{01} mode as 99%. The characteristic nonlinearity length, in this case, is 20 mm, which avoids the energy transfer from the LP_{01} mode into the other higher modes and ensures the parabolic reshaping of the pulse. We should indicate here that, the initial pulse energy is also chosen to give the similar dynamics investigated in the GRIN-F case and discussed in detail in Sect. 3.1. As a result, the pulse evolution in 1 m of STEP-F shows the characteristics of

the self-similar regime, where a decrease in pulse amplitude and a corresponding increase in pulse width, accompanied by a substantial broadening of the pulse spectrum, is evident. The input pulse evolves along the STEP-F towards a parabolic shape with a linear chirp. The corresponding results are similar to those reported for the GRIN-F, and presented in Figs. 1 and 2, respectively. The only difference is that the Gaussian-like spatial beam size in the STEP-F is larger than that of the GRINI-F due to the different mode field diameters of the LP_{01} mode for both MMFs.

4.2 Under the condition of excitation by the equal energy distribution among all the modes

The STEP-F used in this work presents a lower nonlinear coefficient than the GRIN-F so higher initial pulse energy is required to permit pulse reshaping towards the parabolic waveform during its propagation in the fiber. However, using high pulse energy leads to strong nonlinear modes coupling, which directly affects the multimode pulse evolution and the corresponding spatial beam profile as well. To avoid this issue, we have decreased the initial pulse energy and increased the fiber length. To do this, the initial pulse energy of 3 nJ is equally distributed among all the modes and a STEP-F length of 10 m, is used. The corresponding results are depicted in Fig. 5. It is clearly seen that the initial pulse shows significant temporal reshaping and it is break-up into different modes, while all the modes evolved towards the parabolic shapes in both the temporal and spectral domains, as shown in Fig. 5a and b, respectively. The small energy variation observed among all the modes is due to the weak energy transfer that occurs between modes, as shown in Fig. 5d. Note that, degenerate LP_{21} modes, since they travel at the same group velocity, are fully coupled, in which energy transfer between these pairs of modes seems very relevant, then the energy of LP_{21b} mode is transferred into LP_{21a} mode. Note also that, the large modal dispersion in the STEP-F leads to a large walk-off between LP_{01} and LP_{02} modes, which means that the coupling between these modes may be less efficient. However, LP_{02} mode overlaps with LP_{01} at an earlier distance of propagation (at 0.1 m) and leads to energy transfers from LP_{01} into LP_{02} mode. Consequently, Fig. 5b shows clearly the spectral shift induced on the spectrums of these modes due to the XPM effect, since they are traveling at different speeds. The LP_{01} mode shows spectral red-shift, while LP_{02} indicates spectral blue-shift, resulting in speed-up of LP_{02} and slow down of LP_{01} mode, as observed in Fig. 5a. Figure 5c. displayed the evolution of M parameters for all the modes. Unlike the GRIN-F case, the M parameter is evolved in the same manner among all the modes with $M \sim 0.01$. That is because, all the modes propagate with a steady-state of energy evolutions, which makes the parabolic reshaping process stable among all the modes during their propagation. Notably, the small deviation observed in the M parameter evolution of the LP_{01} mode is due to the coupling with the LP_{02} mode at an earlier distance of propagation, as mentioned above. Besides, the spatial beam evolution in the STEP-F is presented in Fig. 6e and f, show that the output spatial beam profile is containing all the modes, where energy transfer between the pairs of modes (LP_{21a} and LP_{21b}) is clearly visible.

Further, we have also investigated the effect of higher initial pulse energy on the energy transfer mechanism between modes in the STEP-F. For initial pulse energy of 30 nJ equally distributed among all the modes, the temporal pulse shape, the output spatial beam profile, and the modal energy evolution, of the six modes, are presented in Fig. 6a and b, respectively. It can be seen that increasing the initial pulse energy leads to a deterioration of modes reshaping towards parabolic waveforms due to the strong energy transfer that

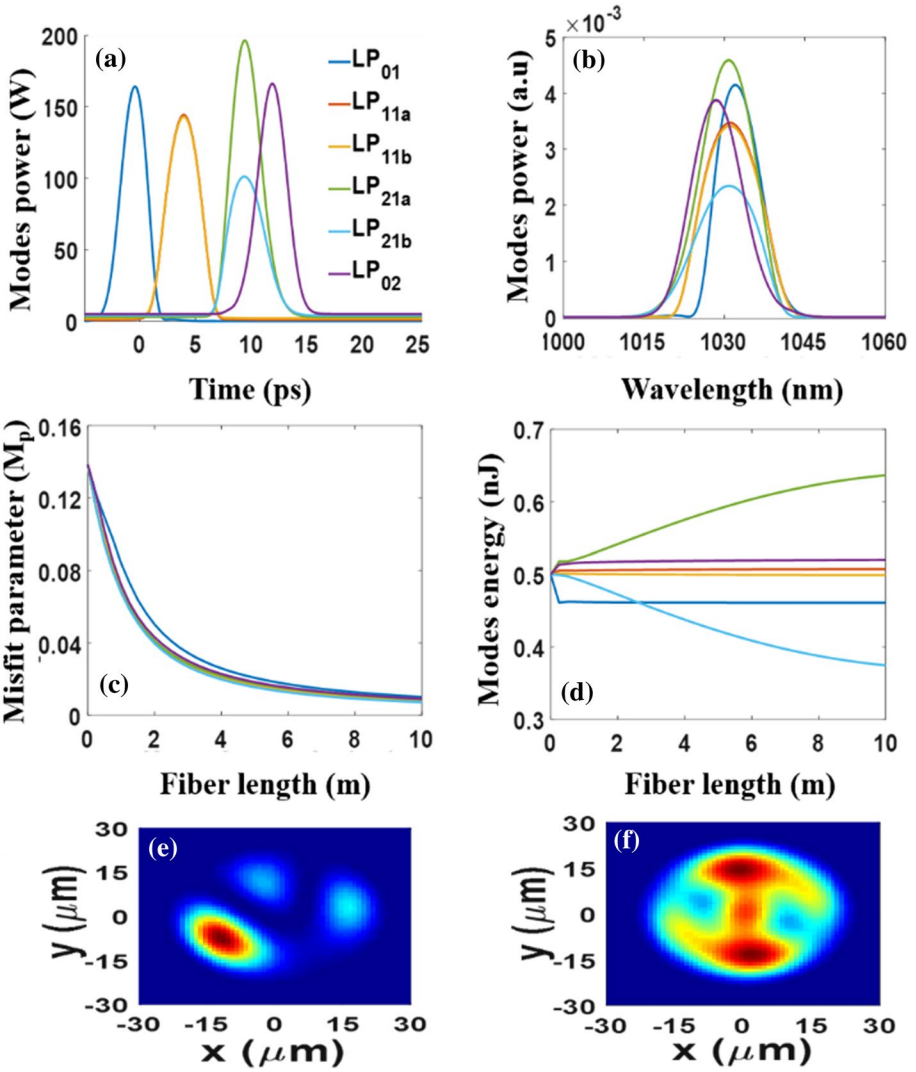

Fig. 5 The output power (**a**), the corresponding spectra (**b**), the misfit parameters (**c**), and the modal energy evolution (**d**) of all the modes. The input (**e**) and output (**f**) spatial beam profiles

occurred between modes, more significantly, between degenerate LP_{21} modes. The most energy is transferred from LP_{21b} into LP_{21a} mode, and so LP_{21a} emerges and dominates with up to 14.5 nJ (~50%) at the fiber output. The LP_{02} mode keeps its initial energy of 5 nJ. Whereas the other modes lost energy with nearly the same amount of ~2–3 nJ. Besides, the output spatial profile plotted in the inset of Fig. 6a is shown to be of the LP_{21a} mode as it is dominated. Consequently, like the GRIN-F case, the parabolic pulse formation process also has a prominent effect on the spatiotemporal behavior inside the STEP-F. In this case, the occurrence of beam auto-selection is observed on the LP_{21a} mode. However, the LP_{21a} mode is dominated beyond the parabolic formation regime.

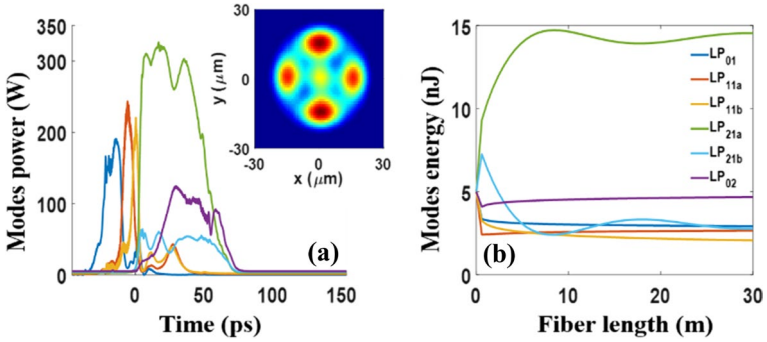

Fig. 6 The output power (**a**), and the modal energy evolutions (**b**) of all the modes. (Inset: output spatial beam profile)

5 Conclusion

In this paper, various numerical simulations are carried out to investigate the spatiotemporal dynamics of parabolic pulses evolution in two kinds of MMFs (GRIN-F and STEP-F). We have used different initial pulse energies, mainly coupled in the fundamental mode, to excite the parabolic pulses generated in the GRIN-F (7 nJ) and STEP-F (50 nJ). The results showed that the initial pulse evolved into a linearly chirped pulse with a parabolic intensity shape, after 1 m of propagation in both MMFs. The parabolic pulse duration (FWHM) and spectral bandwidths are 2 ps and 60 nm, respectively. These pulses are then, compressed to up 40 fs, and a factor of ~ 5 temporal compression is achieved. We have also demonstrated a route to the parabolic pulse evolutions for all the modes when the initial energy is equally distributed among them. In the GRIN-F, owing to the very small walk-off, the modes are well centered in the temporal and spectral domain, and so a localized multimode pulse is achieved for initial energy of 1.5 nJ. It is the worth investigating, that spatial beam autoselection on the LP_{02} mode is observed, since it is dominated when the initial pulse energy is increased up to 15 nJ. This thus offers a very promising way to obtain high beam quality of the generated parabolic pulses on the selected mode. However, the initial pulse energy of 30 nJ is strong enough to cause significant nonlinear modes coupling, and so the shape deterioration of all modes appeared. While in the STEP-F, the large walk-off between modes leads to a pulse break-up into different modes during propagation in 10 m of fiber length, for initial pulse energy of 3 nJ. When the initial pulse energy is increased up to 30 nJ, the modes shape deteriorates, and spatial energy transfer between the degenerate modes LP_{21} is observed. In summary, we can deduce that parabolic pulse shape in passive MMFs is strongly limited by the initial launch conditions. Its stability during the propagation through the fiber is matching properly the parameters of the initial pulse energy. Indeed, to find an optimized design of the proposed configuration, the pulse parameters, such as the initial pulse energy and the MMFs structure, should be chosen judiciously to ensure the formation of a parabolic pulse, and to avoid the undesired intermodal effects. By analyzing spatiotemporal parabolic pulses propagated in MMFs, our study provides a simple framework to understand complicated nonlinear dynamics in MMFs, contributing to applications of multimode fiber lasers. In addition, the potential to obtain a single-mode beam profile can be used for beam delivery applications.

Acknowledgements This work was supported by the Directorate-General for Scientific Research and Technological Development (DG-RSDT) of Algeria and the TURKEY BURSLARI scholarship.

Declarations

Conflict of interest The authors declare that they have no known competing financial interests or personal relationships that could have appeared to influence the work reported in this paper.

References

Ahsan, A.S., Agrawal, G.P.: Graded-index solitons in multimode fibers. Opt. Lett. **43**, 3345–3348 (2018)
Anderson, D., Desaix, M., Karlsson, M., Lisak, M., Quiroga-Teixeiro, M.L.: Wave-breaking-free pulses in nonlinear-optical fibers. J. Opt. Soc. Am. B **10**, 1185–1190 (1993)
Biswas, P., Adhikary, P., Biswas, A., Ghosh, S.N.: Formation and stability analysis of parabolic pulses through specialty microstructured optical fibers at 2.1 μm. Opt. Commun. **377**, 120–127 (2016)
Boscolo, S., Latkin, A.I., Turitsyn, S.K.: Passive nonlinear pulse shaping in normally dispersive fiber systems'. J. Quantum Electron. **44**, 1196–1203 (2008)
Chowdhury, D., Ghosh, D., Bose, N., Basu, M.: Parabolic pulse regeneration in normal dispersion-decreasing fibers and its equivalent substitutes in presence of third-order dispersion. Appl. Phys. B **125**, 106 (2019)
Deliancourt, E., Fabert, M., Tonello, A., Krupa, K., Desfarges-Berthelemot, A., Kermene, V., Millot, G., Barthélémy, A., Wabnitz, S., Couderc, V.: Wavefront shaping for optimized many-mode Kerr beam self-cleaning in graded-index multimode fiber. Opt. Express **27**, 17311–17321 (2019)
Fermann, M.E., Kruglov, V.I., Thomsen, B.C., Dudley, J.M., Harvey, J.D.: Self-similar propagation and amplification of parabolic pulses in optical fibers. Phys. Rev. Lett. **84**, 6010–6013 (2000)
Finot, C., Parmigiani, F., Petropoulos, P., Richardson, D.J.: Parabolic pulse evolution in normally dispersive fiber amplifiers preceding the similariton formation regime. Opt. Express **14**, 3161–3170 (2006)
Finot, C., Provost, L., Petropoulos, P., Richardson, D.J.: Parabolic pulse generation through passive nonlinear pulse reshaping in a normally dispersive two segment fiber device. Opt. Express **15**, 853–864 (2007)
Ghosh, D., Basu, M., Sarkar, S.: Generation of self-similar parabolic pulses by designing normal dispersion decreasing fiber amplifier as well as its staircase substitutes. J. Lightwave Technol. **27**, 3880–3887 (2009)
Hirooka, T., Nakazawa, M.: Parabolic pulse generation by use of a dispersion-decreasing fiber with normal group-velocity dispersion. Opt. Lett. **29**, 498–500 (2004)
Hult, J.: A fourth-order Runge-Kutta in the interaction picture method for simulating supercontinuum generation in optical fibers. J. Lightwave Technol. **25**, 3770–3775 (2007)
Iakushev, S.O., Shulika, O.V., Sukhoivanov, I.A.: Passive nonlinear reshaping towards parabolic pulses in the steady-state regime in optical fibers. Opt. Commun. **285**, 4493–4499 (2012)
Kruglov, V.I., Peacock, A.C., Harvey, J.D., Dudley, J.M.: Self-similar propagation of parabolic pulses in normal-dispersion fiber amplifiers. J. Opt. Soc. Am. B **19**, 461–469 (2002)
Krupa, K., Tonello, A., Couderc, V., Barthélémy, A., Millot, G., Modotto, D., Wabnitz, S.: Spatial beam self-cleaning in multimode fibres. Nat. Photonics **11**, 237–241 (2017)
Krupa, K., Tonello, A., Couderc, V., Barthélémy, A., Millot, G., Modotto, D., Wabnitz, S.: Spatiotemporal light-beam compression from nonlinear mode coupling. Phys. Rev. A **97**, 043836 (2018)
Leventoux, Y., Parriaux, A., Sidelnikov, O., Granger, G., Jossent, M., Lavoute, L., Gaponov, D., Fabert, M., Tonello, A., Krupa, K., Desfarges-Berthelemot, A., Kermene, V., Millot, G., Février, S., Wabnitz, S., Couderc, V.: Highly efficient fewmode spatial beam self-cleaning at 1.5μm. Opt. Express **28**, 14333–14344 (2020)
Liu, Z., Ziegler, Z.M., Wright, L.G., Wise, F.W.: Megawatt peak power from a Mamyshev oscillator. Optica **4**, 649–654 (2017)
Lopez Aviles, H.E.,.Buttolph, M, Wise, F.W., Correa, R.A., Christodoulides, D.N.: Parabolic pulse generation in totally passive tapered multimode fibers. In: Conference on Lasers and Electro-Optics, OSA Technical Digest (Optical Society of America), Paper JW2A.103. (2019)
Mafi, A.: Pulse propagation in a short nonlinear graded-index multimode optical fiber. J. Lightwave Technol. **30**, 2803–2811 (2012)

Poletti, F., Horak, P.: Description of ultrashort pulse propagation in multimode optical fibers. J. Opt. Soc. B Am. **25**, 1645–1654 (2008)
Schukarev, I., Korobko, D., Zolotovskii, I.: Parabolic pulse generation in short fiber amplifiers. J. Opt. **21**, 105505 (2019)
Teğin, U., Ortaç, B.: Spatiotemporal instability of femtosecond pulses in graded-index multimode fibers. IEEE Photonics Technol. Lett. **29**, 2195–2198 (2017)
Teğin, U., Ortaç, B.: Cascaded Raman scattering based high power octave-spanning supercontinuum generation in graded-index multimode fibers. Sci. Rep. **8**, 12470 (2018)
Teğin, U., Kakkava, E., Rahmani, B., Psaltis, D., Moser, C.: Spatiotemporal self-similar fiber laser. Optica **6**, 1412–1415 (2019)
Teğin, U., Rahmani, B., Kakkava, E., Borhani, N., Moser, C., Psaltis, D.: Controlling spatiotemporal nonlinearities in multimode fibers with deep neural networks. APL Photonics **5**, 030804 (2020)
Wen, J., Duan, L., Ma, C., Fan, W.: Numerical simulation and analysis of femtosecond pulse evolution in liquid-core photonic crystal fiber based on adaptive step-size methods. Opt. Quantum Electron. **51**, 184 (2019)
Wright, L.G., Ziegler, Z.M., Lushnikov, P.M., Zhu, Z., Eftekhar, M.A., Christodoulides, D.N., Wise, F.W.: Multimode nonlinear fiber optics: MASSIVELY parallel numerical solver, tutorial and outlook. IEEE J. Sel. Top. Quantum Electron. **24**, 1–16 (2018)
Wright, L.G., Sidorenko, P., Pourbeyram, H., Ziegler, Z.M., Isichenko, A., Malomed, B.A., Menyuk, C.R., Christodoulides, D.N., Wise, F.W.: Mechanisms of spatiotemporal mode-locking. Nat. Phys. **16**, 565–570 (2020)
Zhanwei, L., Wright, L.G., Christodoulides, D.N., Wise, F.W.: Kerr self-cleaning of femtosecond-pulsed beams in graded-index multimode fiber. Opt. Lett. **41**, 3675–3678 (2016)